Oil & Natural Gas Technology

DOE Award No.: DE-FE0013531

FINAL REPORT

Project Title
Assessing the response of methane hydrates to environmental change at the Svalbard continental margin

Project Period (11/1/2013 to 10/31/2018)

Submitted by:

Marta E. Torres

[signature]

and

Frederick Colwell

[signature]

Oregon State University
DUNS #: 053599908
104 CEOAS Admin. Bldg.
Corvallis, OR 97331-5503
Email: mtorres@coas.oregonstate.edu; rcolwell@coas.oregonstate.edu
Phone numbers : (541) 737-2902; (541) 737-5220

Prepared for:
United States Department of Energy
National Energy Technology Laboratory

Report issued on October 15, 2018

U.S. DEPARTMENT OF ENERGY | **NATIONAL ENERGY TECHNOLOGY LABORATORY**

Office of Fossil Energy

DISCLAIMER

Assessing the response of methane hydrates to environmental change at the Svalbard continental margin

ABSTRACT -

This project reflects the results of cooperative research efforts between the US Department of Energy and scientists from Norway and Germany, who collaboratively designed the study, collected and analyzed samples from the water column and sediment and arrive at conclusions presented in joint publications. The main goal of the project was to assess the role of gas hydrate deposits in modulating methane discharge revealed through water column data, and assess the changes in environmental parameters, geochemical and microbiological conditions that drive the methane release in this high latitude region. Samples and data were collected from seven expeditions that encompassed extensive water column surveys, gravity coring, remotely-operated towed instrumentation and seafloor drilling campaigns. Geochemical and microbiological results were interpreted in the context of correlative geophysical data and numerical models, to generate a comprehensive and interdisciplinary view of the processes operating along the Svalbard margin. Incubation experiments complement the filed observations and provide additional data on the microbiological response to methane change. Collectively our results show that methane seepage in this margin is a component of a large methane plume, the Svalbard plume, which is not associated with gas hydrate processes. Consistently, numerical models of data from shallow (gravity cores offshore Storfjordrenna, bearing gas hydrate) and deep (MeBo drilling offshore Prins Karls Foreland) sediment samples show that methane and gas hydrate dynamics at sites that lie within the upper edge of gas hydrate stability are not responding to modern changes in bottom water temperature. Rather the data point to a long history of methane release, dominantly controlled by large scale Earth system changes (*e.g.,* geology, oceanography, and glaciology) with gas hydrate as a temporary methane reservoir. Further results document the episodicity of the methane release, the role of microbes in sequestering methane carbon into authigenic carbonate, reaction networks involved in carbon recycling pathways at the sulfate-methane transition, and response of microbial communities to changes in methane flux allowing for a richer understanding of microbial ecology in response to change at methane seep sites.

TABLE OF CONTENTS

EXECUTIVE SUMMARY

In November 2013, Oregon State University initiated the project entitled: **Assessing the response of methane hydrates to environmental change at the Svalbard continental margin**. In this project, we took advantage of a unique opportunity to collaborate with researchers from Germany (MARUM and GEOMAR) and Norway (CAGE) to collect and analyze samples from the Svalbard continental margin. Water column and sediment samples were collected from three locations along this margin during seven research expeditions. A transdisciplinary strategy that involved seafloor imaging, geochemical and microbiological data, laboratory experiments and modeling approaches led to advanced understanding of processes at play in this high latitude region, specifically the biogeochemical response of changing methane fluxes that is relevant other continental margins.

A comprehensive water column survey, during expeditions HE449 and HE450 (2015) led us to identify a large methane-rich plume along the Hornsund Fracture Zone (HFZ), which marks the continent-ocean boundary of this margin. The plume, which extends from 74° to 79°, was named the Svalbard plume. More than a thousand gas discharge sites were imaged as acoustic flares along the HFZ, which occur in water depths at and shallower than the upper edge of the gas hydrate stability zone. The seep sites surveyed include the area offshore Prins Karls Foreland (PKF), where the first reports of methane discharge were attributed to gas hydrate dissociation by anthropogenic warming by Westbrook et al., (2009). In contrast to this interpretation, our results point to a geologically controlled natural release of methane along the Svalbard margin unrelated to anthropogenic forcing.

Our conclusions are consistent with previous inferences based on the presence of carbonate crusts in this region, which originated >1000yrs ago, i.e. way before onset of anthropogenically-driven climate change. Retrieving sediment samples from the PKF area using conventional gravity cores was proven extremely difficult due to glacial gravel deposits that characterize this region. During expedition MSM057 sediment was sampled using the seafloor drill MeBo from the University of Bremen. No gas hydrate was recovered offshore PKF, and furthermore, modeling of the dissolved chloride data in pore fluids from the drill sites revealed that gas hydrate dissociation occurred in response to isostatic rebound upon retreat of the Barents Sea ice sheet. Not only is the methane release not related to anthropogenic warming, but even during the postglacial isostatic forcing, gas hydrate dissociation did not constitute a major source of methane to the ocean (Wallmann et al., 2017).

In Vestnesa Ridge methane venting has also been occurring over geologic times. Seafloor imaging using a towed-camera tool during a CAGE 15-5 expedition provided first visual evidence of carbonate crusts and surface gas hydrate within the pockmarks where methane is actively discharging (Panieri et al., 2017). Composition of the venting gases measured during this expedition showed a mixture of biogenic and thermogenic gases, consistent with previous published data. Sample collection using the MeBo drill document the origin and transformations of volatiles feeding the gas emissions (Pape et al., 2018). By sampling sediment across

a fault, our data show that gas hydrates are present only when fed by channeled fault migration of thermogenic hydrocarbons. Measured geothermal gradients (~80° km^{-1}) and known formation temperatures suggest that the hydrocarbons are formed at depths >800 mbsf. Using a combined analytical/modeling approach we also document a contribution of microbial methanogenesis to the overall volatile budget that includes a component of secondary carbonate reduction (CR) generated by anaerobic oxidation of methane (AOM) in the uppermost methanogenic zone. Collectivelly, the data presented in Panieri et al (2017) and Pape et al. (2018) show that AOM and CR rates are highest at seep sites, and provide estimates for the amounf of methane being consumed by microbial activity within the sediment. The role of microbes in this setting is being further investigated by analyses of biomarkers (Yao et al., 2018) and microbial communities.

In addition to the results from PKF and Vestensa Ridge, we report on the discovery of a group of mound structures in the Storfjordrenna Trough area. The mounds lie at the edge of gas hydrate stability at ~380 meters water depth; they are ~500 meters in diameter and 10 meters in height, and contain gas hydrate in the shallow subsurface. These mounds were visited and sampled during three CAGE expeditions. Data obtained from gravity and push cores were used to show that the episodicity of the venting regime is not linked to changes in bottom water temperature, but rather responds to dynamics of pressure build-up and release of the methane reservoir (Hong et al., 2017). Changes in fluid composition within nearby sites documented the decoupled methane transport by gaseous and aqueous phases and revealed a three-stage evolution model for active seepage in the region (Hong et al., 2018). We took advantage of this setting to conduct microbial community analyses within the context of geochemical and temporal gradients. This research showed that populations of anaerobic methanotrophs and sulfate-reducing bacteria were highest at seep sites, and that microbial responses are largely synchronous with the advancement of a methane front. Following passage of a methane front the community structure shifted on timescales of years. This is the first combined geo-microbiological study that shows how microbial communities respond to changes in methane flux in natural settings (Klasek et al, 2018). A follow-up laboratory study documents microbial response of samples from different methane regimes, which were incubated under different methane concentrations (Klasek et al., 2018, in prep).

The very productive outcome of this international collaboration is evidenced on seven papers published in highly ranked journals, 3 additional submitted manuscripts, two articles in preparation; two articles published in the Fire in the Ice magazine. In addition the results from this project resulted in more than 15 presentations at science conferences and meetings.

1. INTRODUCTION-

The importance of understanding the role that gas hydrates play in the global carbon cycle and their potential as a future energy resource has long been recognized, and it constitutes an important component of the NETL Gas Hydrate Program. Fundamental questions remain as to the residence time of gas hydrates near the seafloor and deeper within the sediment column, the sources and pathways of methane transport, nature and driving mechanisms for flow, and changes in these variables through time. To answer these questions, we must understand the production and consumption terms of methane and the environmental forcing mechanisms that modulate the relative contributions of various processes that ultimately lead to methane generation, consumption and discharge to the overlying water. The research presented here is focused on characterizing carbon cycling in a high latitude region where the observed release of methane has been attributed to respond to gas hydrate dynamics in a climate sensitive region.

1.1 STUDY AREA

The Norwegian-Svalbard continental margin (Figure 1) is of particular interest to programs aimed at understanding gas hydrate response to environmental change at a high latitude setting. Previous studies in this region have documented the presence of fluid migration in the sediments, submarine mass wasting, normal faulting, hydrocarbon accumulation, sediment fan development, gas hydrate formation, and intensive methane release from the seafloor (Vogt et al. 1999, Vanneste et al. 2005, Hustoft et al. 2009, Westbrook et al., 2009). This high-latitude gas hydrate province is characterized by active faulting, earthquake generation and the presence of a young oceanic crust that drives its high heat flow regime. The predominant lithologies are turbiditic, glaciomarine and hemipelagic sediments, in part reworked by contour currents (Vorren et al. 1998).
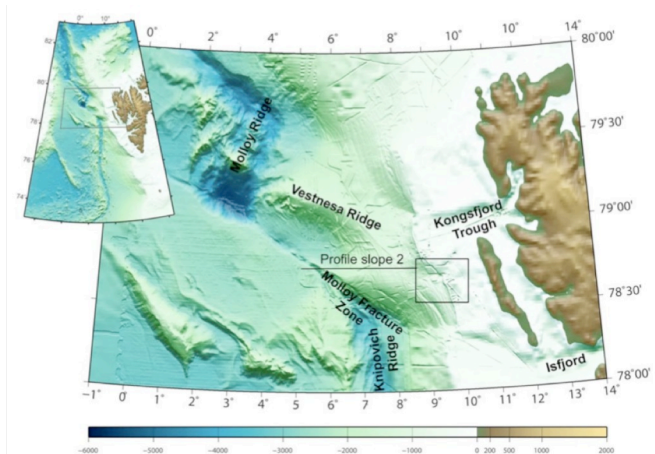
Figure 1 Area of proposed study at the upper continental slope west of Spitsbergen showing the location of Vestnesa ridge and Prins Karls Foreland

The ocean-continent transition has been well imaged by seismic data that reveal a prominent bottom seismic reflection (BSR) corresponding to the predicted base of the gas hydrate stability zone (BGHSZ) (Vanneste et al. 2005). Recent estimates based on seismic data predict hydrate concentrations of up to

11% of pore space in a 90-m thick sediment section above the BSR (Westbrook et al. 2009).

Acoustic data collected in 2008 with the RRS James Clark Ross reveal more than 250 active gas bubble plumes that emanate from the seafloor at water depths shallower than 400 m, the majority of which are located just landward of the UEGHS. This observation led to the hypothesis that the methane discharge here is triggered by a 1° C warming of the northward–flowing West Spitsbergen current over the last 30 years (Westbrook et al. 2009). Although the methane release from gas hydrates due to warming is not yet proved, the implication of the postulated gas hydrate dissociation is significant for a large portion of the Arctic continental slope, because the West-Spitsbergen current feeds into the Arctic Ocean (Westbrook et al. 2009).

West of Svalbard lies the SE-NW to E-W bending elongated sediment drift known as the Vestnesa Ridge (Figure 1), which is characterized by methane plumes and abundant pockmarks on the seafloor (Petersen et al. 2010). Holocene sedimentation here is dominated by muddy-silty contourites with abundant ice-rafted debris (IRD) deposited under the persistent flow of the West-Spitsbergen Current (Howe et al., 2008). A prominent BSR has been documented on seismic data from the Vestnesa Ridge (e.g. Vaneste et al., 2005a). A 1-3 km wide and 50 km long belt of pockmarks on the crest of the Vestnesa Ridge, have been interpreted as the surface expressions of focused fluid- flow structures, which are imaged seismically as acoustic chimneys that pierce through the overburden sediments (Petersen et al., 2010; Bünz et al., 2012). These features likely reflect active methane migration and gas hydrate formation near the seafloor (Vogt et al., 1994), and indeed gas hydrates were recovered from one of the active pockmarks during a cruise in summer 2012. The presence of a BSR and gas hydrate recovery defines this region as one of the northernmost gas hydrate provinces along Arctic continental margins (Hustoft et al., 2009).

2 PROJECT SCOPE AND APPROACH

The main objective of this project was to constrain the biogeochemical response of methane hydrates to environmental change on a high latitude setting (the Svalbard Margin). Specifically we aimed to:

1. Assess changes in chemistry and microbiology across vertical gradients (i.e., within a core) and horizontal gradients (i.e., across the putative upper edge of gas hydrate stability).

2. Use numerical modeling approaches to synthesize the expected response to environmental change of carbon cycling pathways in general and more specifically, processes occurring at the sulfate-methane transition zone (SMTZ).

To this aim, we aimed at constraining: methane sources and transport within the sediment, including mechanisms of gas hydrate formation; cycling of methane by
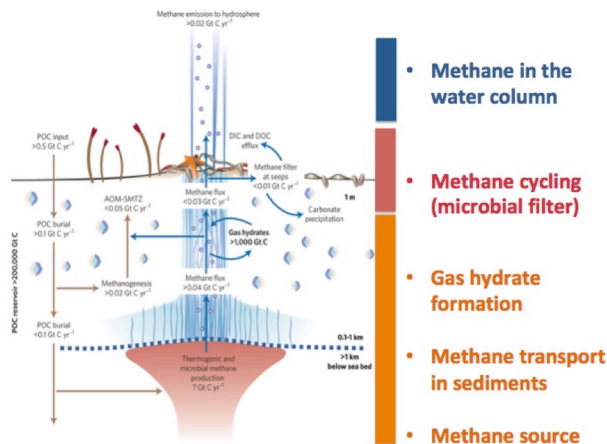
Figure 2. Schematic view of the processes at play in gas-hydrate bearing systems. Modified Boetius and Wenzhöfer (2013)

microbes and the release of methane in the water column, as illustrated schematically in Figure 2.

3. EXPERIMENTAL METHODS:

3.1 NUMERICAL MODELS:

Two different numerical modeling efforts were employed as part of this project: 1) A reduced numerical model was developed for methane hydrate formation under conditions of variable salinity; and 2) Kinetic-transport reaction models were used to investigate the gas hydrate and microbiological responses to changes in temperature and methane fluxes.

3.1.1 Computational model of methane hydrate formation in variable salinity conditions. We develop a reduced model for methane hydrate formation in variable salinity conditions and provided details on the equilibrium phase behavior adapted to a case study from Ulleung Basin. One of the advantages of this reduced model, in contrast to fully comprehensive models, is that the reduced model is easy to implement and to extend, and is amenable to various analyses. The two-phase three-component model is very robust and efficient as well as amenable to various numerical analyses, yet is capable of simulating realistic cases. We give details on application of our model and compare various thermodynamic models for equilibria. Whereas at seawater values these models and data are very consistent, at salinites higher than seawater we observed significant inconsistencies among the various theoretical predictions. The best fit to laboratory data was achieved with the Sloan and Koh (2008) model. We then incorporated the hydrate stability and saturation prediction of Sloan and Koh (2008) into our numerical model to simulate the dilution-corrected pore water Cl profiles from Ulleung Basin and confirm the significance of advective migration of gaseous methane below the methane hydrate stability zone. In a follow-up paper we described the computational aspects of the model, with the emphasis placed on the variants of time-stepping. Our reduced model accounts for three components: water, methane, and salt, and two phases: aqueous, and solid (hydrate). Results from these modeling efforts are published in Peszynska et al. (2015 a, b)

3.1.2 Kinetic Transport-Reaction models- To model pore water profiles we the FORTRAN routine CrunchFlow (Steefel et al., 2014) was coupled with a custom MATLAB routine to simulate different biological, hydrological, and geological processes that may impact the porewater geochemistry in the Svalbard margin as

described in various publications resulting from this project (Hong et al., 2016, 2017, 2018; Pape et al., 2018).

For example, our 1-D transport-reaction model described in Hong et al., 2017, simulates a sediment column considering diffusion of dissolved methane and sulfate in addition to the consumption of both species by anaerobic oxidation of methane (AOM). We consider only fluid phase in our model (*i.e.*, no solid and gas phases). The governing equations are:

$$\frac{\partial C}{\partial t} = -\frac{1}{\phi}\frac{\partial F}{\partial x} + R_{AOM} \quad (1)$$

$$F = -\phi D_s \frac{dC}{dx} \quad (2)$$

where *f*, D_s and $\frac{dC}{dx}$ are sediment porosity (0.6), diffusion coefficient in porous media, and concentration gradient for the two target species, *t* is time in years, *x* is depth in meters below seafloor (mbsf), *C* is the concentration of porewater species in mole/m³ (volume of bulk sediments), and R_{AOM} is the AOM reaction rate in mole/m³/yr. Diffusion coefficients for seawater media (*D*) were calculated with temperature set to be the bottom water values (0.56 °C) measured during CTD casts in May 2015. We estimated 0.0158 and 0.0301 m²/yr for the diffusion coefficients of sulfate and methane, respectively. No available information for tortuosity (θ) in this area limits the accuracy of our model results. To at least constrain the order of magnitude of our age estimation, we ran the model with tortuosity of 1.5 and 2.2, a range that covers the possible tortuosity for clayey sediments with 0.6 to 0.7 porosity. These tortuosity values were then used to define diffusion coefficients in porous media (D_s) following:

$$Ds = \frac{D}{\theta^2} \quad (3)$$

We derive the initial conditions of the model by progressing the model until sulfate profiles match the shallow part of the profiles at each site. We use no flux boundary as the lower boundary condition for sulfate. Fixed methane concentrations were assigned at the bottom of the model frame as boundary conditions.

We did not include fluid advection induced by sediment burial and compaction as the measured porewater chloride content and porosity profiles show very little reduction with depth. It is likely that the advection of fluid due to pressure difference between gas reservoir at depth and surficial sediments may accelerate the transport of dissolved methane, which we are not able to constrain with the available data. We solved Eq. (1) numerically by discretizing depth using a centered forward finite difference scheme and time using an implicit Crank-Nicholson scheme. The depth and time discretization (*dx*=0.025 meter for all three sites; *dt*=0.01 for 1520GC and 911GC; *dt*=0.025 for 940GC due to the long modeling time)

were determined by running the model with progressively smaller discretization until the results were numerically stable and accurate.

We solved the R_{AOM} term in Eq. (1) explicitly as:

$$R_{AOM} = R_{AOM}^{max} \frac{C_{SO_4}}{C_{SO_4} + k_{half-SO_4}} \frac{C_{CH_4}}{C_{CH_4} + k_{half-CH_4}} \quad (4)$$

Where $k_{half-SO_4}$ and $k_{half-CH_4}$ are the half saturation constants for sulfate (0.5 mole/m³) and methane (5 mole/m³), respectively. R_{AOM}^{max} is the theoretical maximum AOM rate which we obtained by fitting the sulfate profile (2 mol/m³/yr). The magnitude of this value affects only the shape of profiles close to the sulfate-methane transition (SMT) depth but not the rate of SMT migration. We assumed that AOM is the only diagenetic reaction involving sulfate and methane consumption in this first order simulation; sulfate consumption and methane production due to organic matter degradation were assumed to be not significant under the time scale investigated as these reactions are not likely to induce the dramatic change in porewater concentration gradients. There are two freely-adjusted parameters in this model: boundary condition for methane concentration and the time since the inferred methane pulse initiated. The magnitude of methane flux required was constrained both by the curvature of the sulfate profiles and depth where gas hydrates and/or gas micro-fractures first appear. The methane flux has to be great enough to simulate AOM that can outcompete sulfate diffusion from seafloor. A methane flux that is too small will result in a sulfate profile that lacks the kink structure as from the observed profiles. The methane concentration at the depth of first hydrate appearance, which should equal to methane solubility, is an additional and independent constraint for the modeled methane profile. With methane flux being constrained, we can estimate the duration of the methane pulse required to fit the data.

Figure 3 R/V Helmer Hensen in Longyearbjern (Svalbard), prior to expedition CAGE15-5, May 2015

3.2 FIELD CAMPAIGNS

We collected samples for this project during seven expeditions to the Svalbard margin, as listed in Table 1, all of which took part in collaboration with German and Norwegian scientists (Figure 3).

Table 1- Field campaigns

Research vessel	Exp #	Dates	Leading institution
Helmer Hensen	CAGE14-10	Oct 2014	CAGE
Helmer Hensen	CAGE15-2	February 2015	CAGE
Helmer Hensen	CAGE15-5	May 2015	CAGE
RV Heincke	HE449	July 2015	MARUM
RV Heincke	HE450	Aug.-Sept 2015	MARUM
Helmer Hensen	CAGE16-5	June-July 2016	CAGE
M.S. Merian	MSM 057	Sept-Oct 2016	MARUM

3.3 WATER COLUMN INVESTIGATIONS

3.3.1 Hydroacoustic Profiling.
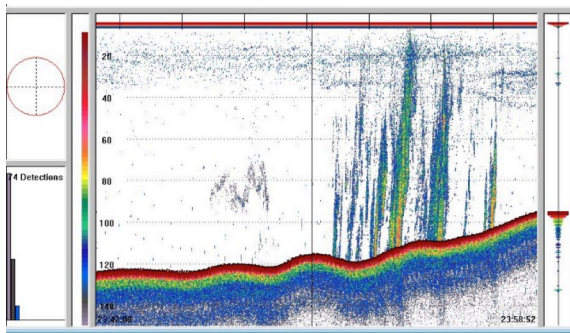
Figure 4. Example of active flare emissions observed by water column hydroacoustic surveys during expeditions HE449 and HE450 (Mau et al., 2017)

Sub-seafloor structures were imaged with the sediment echosounder Innomar SES-2000 medium permanently installed on the hull of the RV Heincke. The system operates at a primary frequency of 100 kHz and we chose a secondary frequency of 6 or 8 kHz. Active gas emissions (Figure 4), which become visible as flares in water column echograms, were recorded with both a split beam echosounder Simrad EK60 with 38 kHz frequency and a Kongsberg EM710 multibeam echosounder operating at a frequency of 70–100 kHz. For the precise localization of individual flares, the water column data were post-processed using the Fledermaus tools. Seafloor origins of individual flares were identified as points of highest amplitudes near the seafloor. The coordinates of these points were extracted using the FMGeopicker and subsequently plotted on top of the bathymetry using ArcGIS10.2. For visualization of flare deflections and bubble rising heights, selected flares were extracted from the water column records of the multibeam echosounder as point data, and were edited using the 3D Editor of Fledermaus. Details are given in Mau et al., (2017).

3.3.2 Water column sampling.

Seawater was sampled using a rosette equipped with 12 ~ 5 l Niskin bottles mounted on a frame that holds a Sea-Bird SBE 911 plus and a SBE 43 oxygen sensor for online monitoring of salinity, temperature, pressure, and dissolved oxygen.

During HE449 and HE450 we sampled twelve water depths at each station for methane concentration analysis. Methane concentration measurements were

performed using the Greenhouse Gas Analyzer 'Enhanced Performance' with 'Syringe Injection Mode' manufactured by Los Gatos Research (LGR), California. The instrument uses conventional laser absorption spectroscopy, where the absorption of the infrared laser beam directed through the sample is used to calculate the mole fraction of methane in the gas. We used three stock standards (1, 10 and 100 ppm methane) and dilutions of these standards to calibrate the instrument in the range from 0.07 to 100 ppm. Water samples were collected by filling two 140 ml syringes, each outfitted with a valve, directly from the Niskin bottles. The syringes were flushed and filled with 100 ml of seawater without any air bubbles. The syringes were left to equilibrate to room temperature or the temperature of the sampled water was measured to avoid a long equilibration time in the case of low temperatures (<5C). A headspace was generated in each syringe by drawing 40 ml of Zero Air into the syringe. Syringes were shaken vigorously for over 1.5 minutes to allow for equilibration between water and headspace. The combined gas volume of 80 ml was injected in the GGA followed immediately by 60 ml injection of Zero Air, which is needed to reach the required volume of 140 ml in the instrument chamber of the GGA.

The GGA calculates methane concentrations based on its internal calibration. To minimize potential errors caused by shifts in the internal calibration of the instrument we ran calibration curves for each batch of samples analyzed. The dissolved methane concentration in the samples was calculated according to the headspace formulation detailed in Magen et al. (2014) and the required Bunsen coefficient was calculated based on the salinity and temperature of the sample. The reproducibility of the method is <2.5%.

### 3.3.3 Stable carbon isotope composition of methane.

From water, collected 1–11 m above seafloor using the CTD-rosette, gas was extracted and analyzed for the stable isotope composition of methane. The stable carbon isotope analysis was performed with an isotope ratio mass spectrometer (IRMS; Finnigan Delta XP plus) at the Alfred Wegener Institute, Bremerhaven, Germany. To concentrate the methane for analysis, the gas was purged and trapped with PreCon equipment (Finnigan). All isotopic ratios are presented in the δ notation against the Vienna Pee Dee Belemnite (VPDB) standard and have an analytical error of <1‰.

3.3.4 Methane oxidation rates.

Methane oxidation (MOx) rates were determined during HE449 from ex situ incubations of water samples in 120 ml serum vials. Sample collection and incubation were performed as described in Bussmann et al. (2015). Briefly, triplicate samples were collected and 100 μl of 3H-labeled methane (~200 kBq) in N_2 were added to each sample. After shaking the bottles to equilibrate the tracer with the water, the samples were incubated in the dark for 48 h at 2.5C. Incubation was stopped by adding 0.3 ml of 25% H_2SO_4. Then the total activity in an 3 ml aliquot was measured by liquid scintillation counting; the activity of ^3H-H_2O was measured after sparging the sample for 30 min with air to remove excess ^3H-CH_4, so

that the net amount of ^{3}H-CH$_4$ consumption can be estimated. Counting was performed on board with a Hidex scintillation counter.

3.4 SEAFLOOR IMAGERY
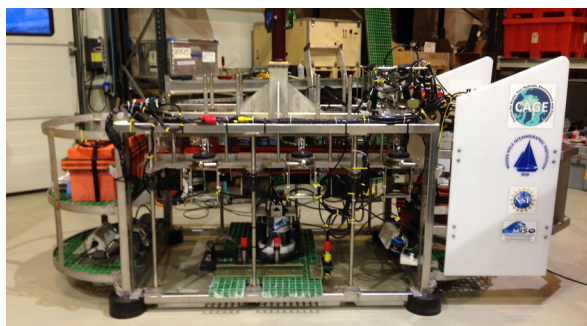
Figure 5. Modified TowCam system used during expedition CAGE15-5 to observe the seafloor and collect water and multicore samples. Details in Panieri et al., 2017

Visual seafloor observations were made during the CAGE15-5 expedition, using a modified TowCam deep-sea imaging system (Figure 5; Fornari, 2003). The TowCam system was developed at the Woods Hole Oceanographic Institution's (WHOI) Multidisciplinary Instrumentation in Support of Oceanography (MISO) Facility. It is equipped with a 16 megapixel deep-sea color digital camera and a real-time Conductivity, Temperature, Depth (CTD) instrument, and an altimeter (http://www.whoi.edu/main/instruments/miso), with real time transmission of images and data. For this study, the TowCam was integrated with the UiT-NPI (UiT - The Arctic University of Norway and NPI - Norwegian Polar Institute) multi-corer. The combined TowCam-Multicorer system (TC-MC) was used to visually survey and sample sediments from the Lunde and Lomvi pockmarks. High-resolution images were collected in order to describe seafloor textures and indicators of fluid activity, identify areas with chemosynthetic fauna and authigenic carbonates, and select sampling targets.

To facilitate geological and biological observations, TowCam-Multicore (TC-MC) imagery was first processed to correct for variations in illumination. The corrected images where then used to identify matching points where overlap between images existed, and to re-navigate the camera positions. Georeferenced photomosaics were generated from the re-navigated images, and then projected and blended to remove image seams and correct for differences in color (Panieri et al., 2017).

3.5. SEDIMENT SAMPLING

Sediment samples were collected using gravity cores and the TC-MC system that allowed for the collection of six 60 cm-long, real-time visually-guided cores (Panieri et al., 2017). In addition, during expeditions MSM057-1 and MSM057-2 we retrieved sediment using the sea-floor drilling rig (MeBo70). This seafloor drill can be deployed from research vessels to retrieve sediments from depths of 70 mbsf (Freudenthal and Wefer, 2013). The central parts of the drill are the drill head and the feeding system. The drill head is a rotary unit that provides the required torque and rotation speed for rotary drilling and for making or breaking the threads of the drill string. Cores are taken from the sea floor by simple pushing a push core barrel

Figure 6. MeBo drilling system being deployed. This system was used during MSM057 expeditions in 2016

(push coring suitable for soft sediments) or by rotating and pushing a rock barrel (rotary drilling for hard rocks). A water pump provides sea water for flushing the drill string for cooling of the drill bit and for removing the drill cuttings. After drilling a 2.5 m section the core is recovered using a wire that is latched to the inner core barrel with an overshot. The outer drill string stays in the drilled hole during the entire drilling process. Therefore no casing is required and drill string handling time decreases drastically.

During expeditions MSM57-1 and -2 in 2016 sediment, from Prins Karls Foreland and Vestnesa Ridge was sampled to a depth of 62.5 mbsf with the seafloor drill rig MARUM-MeBo70 (Freudenthal and Wefer, 2013). Pressurized sediment cores were also recovered with the MeBo pressure core barrels, called MDP (German for MeBo-Druckkern-Probennehmer (Pape et al., 2017).

3.6. PORE WATER ANALYSIS

Porewater samples were extracted at ~4 ^{o}C from both multicores and gravity cores immediately after core recovery using acid-washed rhizon samplers. The samples were collected in 20 ml acid washed syringes and subsequently filtered through 0.2 mm cellulose acetate in-line filters. Before subsampling, the porewater was stored at room temperature for ~15 minutes to allow for temperature equilibration. Subsamples were preserved for shorebased analyses of sulfate by adding 6 ml of a 23.8 mM $Zn(OAc)_2$ solution less than 30 minutes after the syringe was disconnected from the rhizon. Samples for SO_4/HS measurements were stored in -4 ^{o}C freezer until analysis.

For sulfate analyses, we used a Dionex ICS – 1100 Ion Cromatograph outfitted with an AS-DV autosampler and an IonPac AS23 column (eluent: 4.5 mM Na_2CO_3/0.8 mM NaHCO3, flow: 1ml/min). The relative standard deviations from repeated measurements of different laboratory standards are better than 0.5% for concentrations above 0.1 mM and better than 1.8% for concentrations above 0.02 mM.

Dissolved iron was determined spectrophotometrically onboard using a ferrospectral complex in ascorbic acid (1%) at wave length 565 nm. Calibration curves were prepared from iron sulfate standards (10 points from 0.067 to 1 mg/L Fe^{2+}) and determined prior to each sample batch. Standard and ferrospectral solutions were prepared daily with anoxic 18.2 MW MilliQ water using acid-washed volumetric flasks. Measurements were done within an hour after the water samples were extracted.

Concentrations of SHS were analyzed by the "Cline method" (Cline, 1969) after the cruise. Porewater samples fixed with $Zn(OAc)_2$ were well mixed prior to analyses. 50 to 200 ml of sample were diluted to a proper range for the analyses. 10-15 minutes after mixing the samples with the color reagent (N,N-Dimethyl-p-phenylenediamine sulfate salt and $FeCl_3+6H_2O$ dissolved in cool 18.5% reagent grade HCl), they were measured spectrophotometrically with a wave length of 670 nm. Na_2S standard was made fresh every day before analyzing samples. 13 standards with concentrations range from 0.04 to 0.25 mM were made for calibration.

Total alkalinity was measured by Gran titration method a couple hours after the water samples were collected. The HCl titrant (0.012M) was made fresh before the cruise. Before each batch of analyses, 0.01M borax standard and local seawater were titrated for quality control. Titration was performed in an open beaker with constant stirring. The amount of acid and pH was manually recorded during each acid addition. Alkalinity was calculated from the Gran function plots.

Concentrations of major and minor ions were measured by the ICP-OES (Leeman Labs Prodigy) in the W.M. Keck Collaboratory for Plasma Spectrometry at Oregon State University in the radial viewing modes. Samples were diluted 100 times with 1% quartz-distilled nitric acid prior to analyses. Repeated IAPSO and in-house standard were measured for every 11samples to assess the instrumental accuracy and precision. Mean concentrations and 1-sigma uncertainties were calculated from three replicate analyses.

Porewater samples for cation analyses (<6 mL) were acidified onboard with 10ml of 69% ultrapure grade nitric acid which lowered pH to <2. Prior to analyses, the porewater samples were diluted 20-fold with 1% quartz-distilled nitric acid. Repeated IAPSO and an in-house standard were measured every 11 samples to assess accuracy and precision of the measurements (accuracy: Li<2.8%, Sr<3%; precision: Li<1.3%, Sr<1.3%, n=12). A 30 ml aliquot of the acidified subsample was dried and brought up to 75 ml of 3M HNO_3 in preparation for porewater $^{87}Sr/^{86}Sr$ analyses. The samples were then passed through Eichrom "Sr-spec" chromatographic columns to isolate strontium. $^{87}Sr/^{86}Sr$ ratios (at 30 ppb) were measured with a Nu Plasma multicollector inductively coupled plasma-mass spectrometer (MC-ICPMS) in the W.M. Keck Collaboratory as described in Joseph et al. (2012.2013).

Concentrations of ammonium were determined by a colorimetric method with a Technicon AutoAnalyzer II™ component at Oregon State University. The analytical detail is documented in the EPA Criteria "EPA 600/4-79-020 Methods for Chemical Analysis of Water and Wastes".

Subsamples collected at sea for the stable carbon isotopic compositions of dissolved inorganic carbon (DIC) were preserved with mercuric chloride and analyzed shorebased at Oregon State University using a GasBench II automated sampler interfaced to a stable isotope mass spectrometer (Finnigan DELTA Plus XL) (Torres et al., 2005). The overall precision and accuracy is estimated to be better

than ± 0.15‰. Primary standardization is provided by tank CO_2 (referenced to an array of international standards) and analyses are monitored against a stock solution of reagent $NaHCO_3$.

3.7 GAS ANALYSES

All gas samples were analyzed onboard by gas chromatography (GC) for their molecular composition or for ex situ concentrations of methane (Pape et al., 2010). Samples prepared according to the headspace technique yielded relatively low hydrocarbon concentrations and were used only for profiling of ex situ methane concentration, whereas hydrate-bound gas, void gas, and sedimentary gas from the MDP allowed for quantification of C_1 to C_6-hydrocarbons and for calculation of molecular hydrocarbon composition (C_1/C_{2+} ratios).

For molecular characterization, light hydrocarbons (C_1 to C_6) were separated, detected, and quantified with a capillary column connected to a Flame Ionization Detector, while O_2, N_2, CO_2 as well as C_1- and C_2-hydrocarbons were determined using a stainless steel column packed with mole sieve and coupled to a Thermal Conductivity Detector. Calibrations and performance checks of the analytical system were conducted regularly using commercial pure gas standards and gas mixtures. The coefficient of variation determined for the analytical procedure is lower than 2%.

### 3.8 MINERALOGY AND STABLE CARBON ISOTOPES OF CARBONATES

Carbonate samples were powdered and homogenized. Mineralogical analyses were performed by X-ray diffraction (XRD) on un-oriented samples scanned by a Bruker D8 Advance diffractometer (Cu K_a radiation in 3-75° 2q range). Quantitative data were obtained with the Rietveld algorithm-based code, Topas-4, provided by Bruker. Following a displacement correction of the spectrum made on the main quartz peak, the d_{104} displacement of calcite was used to estimate the $MgCO_3$ in mol%[36].

An aliquot of the powder prepared for XRD was used for stable carbon and oxygen isotopic measurements using a GasBench II preparation line connected to a Thermo Scientific Delta V Advantage IRMS (Thermo Fisher Scientific). Carbon dioxide was produced by the reaction of the powdered sample with 103-105% concentrated phosphoric acid at 70°C over 2 hours. Reproducibility is better than ± 0.15 ‰ for $d^{13}C$ values. Stable isotopic compositions are reported in conventional delta (d) units relative to Vienna Pee Dee Belemnite (VPDB) reference.

3.9 MICROBIOLOGY INCUBATIONS

A hand pump was used to hydrostatically pressurize a customized Benthos pressure vessel to 4 MPa, approximating *in situ* pressure (Fig. 7). Briefly, sediment samples were homogenized and 2 g sediment and 8 ml anoxic artificial seawater media (2 mM HCO_3^-, 1.5 mM HS^-, 10 mM SO_4^{2-}) were added to cutoff hungate tubes

in an anaerobic glove bag. Methane (0, 1.5, or 5 mM) was added using gastight syringes. Tubes were placed in the Benthos vessel, pressurized to allow methane to dissolve completely and instantly, and incubated at 4°C for one, four, or nearly eight months. Media for four- and eight- month incubations was sampled once or twice during incubation, respectively, before replacing with fresh media and methane.
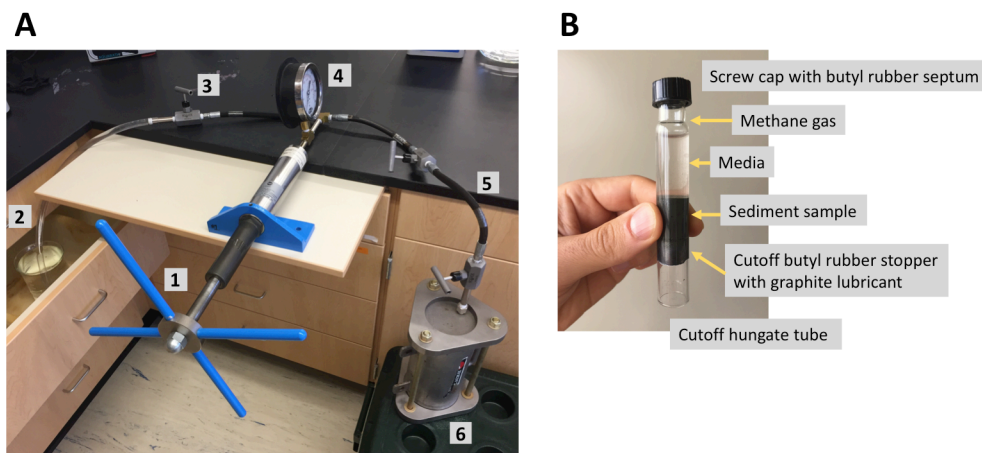
Figure 7. Laboratory high pressure incubation setup (A) and incubation tubes (B). In the incubation setup (A), a hand pump (1) draws water (2) into its barrel. A valve (3) is tightened, and turning of the hand pump increases hydrostatic pressure as registered by a gauge (4). Additional tubing and valves (5) can be used to control pressure entering the customized Benthos vessel (6), where incubation tubes are placed upside-down. Incubation tubes (B), shown right-side up, are cutoff glass hungate tubes containing a slurry of sediment and anoxic seawater media, and methane gas. Butyl rubber septa are used to anoxically add methane gas and sample media. Pressurization of the vessel pushes in the cutoff butyl stoppers, fully and immediately dissolving methane gas into the slurry.

Before measurement, sulfide was preserved using a saturated zinc acetate solution, and dissolved inorganic carbon poisoned with mercuric chloride. Sediment slurries were transferred to 15 ml falcon tubes, centrifuged, supernatant poured off, and pellets frozen at -80°C.

3.10   MICROBIOLOGY

3.10.1 DNA Extraction, Amplification, Sequencing, and Analysis DNA was extracted from sediments in a clean laminar flow hood using a Qiagen DNeasy PowerSoil kit following the manufacturer's protocol. The Earth Microbiome Project 16S Illumina Protocol was used to prepare amplicons for sequencing. Briefly, V4 regions of bacterial and archaeal 16s rRNA genes were amplified in triplicate 25 ul reactions using universal 515-forward and 806-reverse primers modified with dual-indexed Illumina sequencing adapters (Kozich et al., 2013). The thermal cycling protocol of Caporaso et al 2011 was followed without modifications.

After confirming amplification with agarose gel electrophoresis, triplicate PCR products were pooled and purified with a Qiagen QIAquick PCR purification kit. Amplicon concentrations were quantified with a Qubit fluorometer using the Qubit

dsDNA high sensitivity assay kit and pooled in equimolar amounts. Illumina Miseq V2 paired-end 250 bp sequencing was performed by technicians at Oregon State University's Center for Genome Research and Biocomputing (CGRB). Two sediment-free DNA extraction blanks were amplified and included in the sequencing run.

16S gene sequences were processed with mothur (Schloss et al., 2009) following an established pipeline (Kozich et al., 2013). Reads were clustered into OTUs at a 97% similarity level and taxonomically classified using the SILVA database (Quast et al., 2013). Sequences representing potential contaminants previously reported in DNA extraction kits (Salter et al., 2014) and present in sediment-free DNA extraction blanks were removed. Sequences from the genus *Brachybacterium* were also removed, which represented 10% of reads from one of the extraction blanks but only 0.06% of the total reads in the dataset. After removal of singleton OTUs, communities were rarefied to 3,622 reads and relative abundances were calculated. Alpha diversity metrics (number of OTUs, Chao1, Shannon, and Simpson indices) were then determined. To compare beta diversity, a tree file containing the most common individual sequence from each OTU was constructed using clearcut (Evans et al., 2006), and weighted unifrac (Lozupone et al., 2007) distances were calculated from the untransformed OTU table. Weighted unifrac distance files were generated for each set of samples tested for differences in community structure using AMOVA (Excoffier et al., 1992). Metastats (White et al., 2009) was used to determine whether individual OTUs were differentially abundant between groups of samples.

3.10.2 Droplet Digital PCR (ddPCR) was used to quantify abundances of functional genes *dsrAB* and *mcrA* using primer pairs described by Kondo et al. (2004) and Luton et al. (2002), respectively. Reactions of 22 ul volume were prepared in a clean PCR hood in 96-well plates using 1x Bio-Rad QX200 ddPCR EvaGreen Supermix, 200 nM primers, and and 0.88 ul of tenfold-diluted genomic DNA. Droplets were generated on a QX200 AutoDG Droplet Generator using automated droplet generation oil for EvaGreen Supermix (Bio-Rad). Thermal cycling was performed immediately afterwards on a Veriti 96-well thermal cycler. Protocols began with a single initialization step at 95℃ for 5 minutes and then proceeded to 40 cycles of denaturation at 95℃ for 30 seconds, annealing for 1 minute (at a temperature of 53 for *mcrA* and 58 for *dsrAB*), and for *mcrA* only, an extension at 72℃ for 75 seconds. Signal stabilization steps (4℃ for 5 minutes, then 90℃ for 5 minutes) were then performed before maintaining a 4℃ hold. To ensure uniform heating of all droplets, the ramp rate for all amplification cycles was set to 2℃/minute. Reactions were kept at 4℃ overnight and read with the Bio-Rad QX200 Droplet Reader the following morning. Droplet generation and reading were performed by the lead author at OSU's CGRB core facility.

Normalization was performed by inspecting fluorescence distributions using Quantasoft software (Bio-Rad). Threshold fluorescence values were manually imposed by visually inspecting distributions of DNA extraction blank and no-template-added control samples. Amplicon copy numbers per well were then converted to copies per gram wet sediment.

4. RESULTS AND DISCUSSION

The majority of the results presented below have been published in peer-reviewed journals, so here we limit this report to a brief summary of the major findings and direct the reader to the published articles.

4.1 WATER COLUMN INVESTIGATIONS

Numerous articles have recently reported on gas seepage offshore Svalbard, because the gas emission from these Arctic sediments was thought to result from gas hydrate dissociation, possibly triggered by anthropogenic ocean warming. In Mau et al. (2017), reported findings of a much broader seepage area, extending from 74° to 79°, where more than a thousand gas discharge sites were imaged as acoustic flares. The gas discharge occurs in water depths at and shallower than the upper edge of the gas hydrate stability zone and generates a dissolved methane plume that is hundreds of kilometer in length. Data collected in the summer of 2015 revealed that 0.02–7.7% of the dissolved methane was aerobically oxidized by microbes and a minor fraction (0.07%) was transferred to the atmosphere during periods of low wind speeds. Most flares were detected in the vicinity of the Hornsund Fracture Zone, leading us to postulate that the gas ascends along this fracture zone. The methane discharges on bathymetric highs characterized by sonic hard grounds, whereas glaciomarine and Holocene sediments in the troughs apparently limit
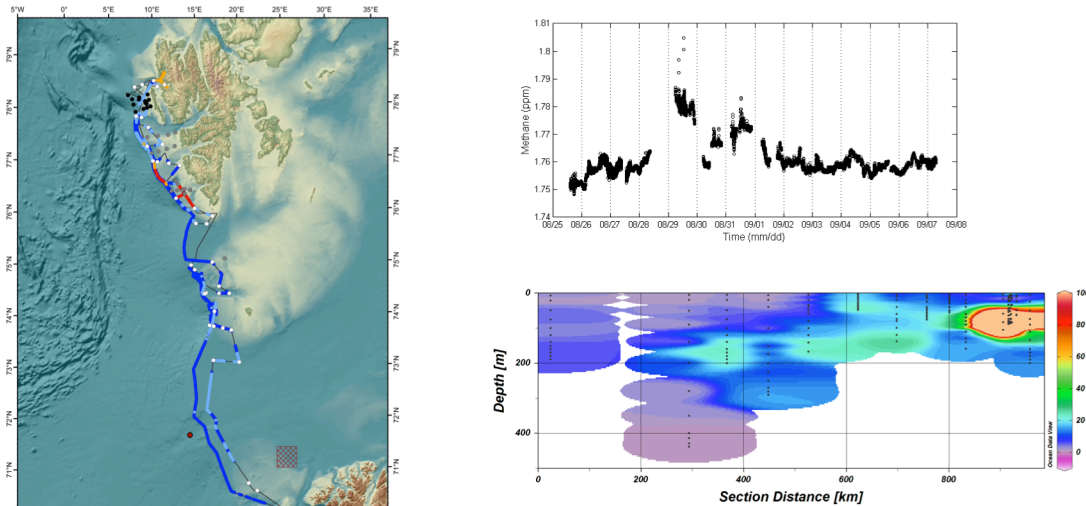
Figure 8A CTD stations of cruises HE387(black), HE449(gray), and HE450(white).The line marks the cruise track of HE450, along which atmospheric methane concentrations were measured(shown in Figure 8B) The color code is: dark blue <1.76ppm, blue 1.76-1.77ppm, orange 1.77-1.78ppm, and red>1.78ppm.

Figure 8B. Methane concentrations of air measured during cruise HE450 Elevated concentrations were measured crossing Hornsundbanken (08/29) and near Kongsfjorden (08/31). **C**. South–North transect of dissolved methane concentrations close to land showing enhanced values below the upper limit of gas hydrate stability. Methane anomaly was derived by subtracting the atmospheric methane equilibrium according to the temperature and salinity of the water sample (2.6-3.5nM). (From Mau et al., 2017a,b)

seepage. We conclude that the large scale seepage reported here is not caused by anthropogenic warming.

4.2 VESTNESA RIDGE

Investigations at the Vestnesa Ridge over the past decade have established the presence of a high density of pockmarks and persistent gas emissions at the seafloor. A regional bottom-simulating reflector substantiates the presence of gas hydrates and free gas at depth. Observations of methane seepage in this area have been reported since 2008.

The first high-resolution deep-sea camera images showing carbonate formation at seafloor pockmarks along the 1200 m deep and 100 km long crest of the Vestnesa Ridge were obtained during cruise CAGE15-5, and reported in Panieri et al., 2007. This paper summarizes and integrates the available information to date and report on the first detailed seafloor imaging and camera-guided multicore sampling at two of the most active pockmarks along Vestnesa Ridge, named Lomvi and Lunde. Widespread authigenic carbonate formations were observed only inside pockmarks, confirming gas expulsion is preferentially concentrating in gas chimneys underlying seafloor pockmarks. Similar to reports offshore Prins Karl Foreman (Brent et al., 2014), the extensive authigenic carbonate deposits discovered in Vestnesa Ridge represent an important and prolonged methane sink, preventing much of the upwardly flowing methane from reaching the overlying ocean.

To better understand the sources, migration pathways and carbon cycling processes in this region, cores collected with the deep sea drill rig MARUM-MeBo70 during the expedition MSM57 in 2016, sampled the deeper sediment section (up to 62.5 mbsf) from the Lunde pockmark; as detailed in Pape et al., 2018. Geochemical data were used to characterize the different fluid regimes, with lowest fluxes at a reference station, intermediate at a non-seep site within the pockmark and highest at two sites drilled at sites of active seepage. At the reference site, the deepest gas sample (62 mbsf) has a major component of migrated thermogenic hydrocarbons. The thermogenic gas migrates originate from deeply-buried (>800 mbsf) Miocene source rocks and are channeled upward thought a deep-rooted fault that intersect the drilled sites at 6–8 mbsf. Shallow gas hydrates at sites of active seepage precipitate from these thermogenic hydrocarbons and the hydrate-bound hydrocarbons are representative for the gas chemical properties of the deeply buried source. Sediments shallower than ca. 50 mbsf show a prevalence of microbially-generated methane. Some of this methane is derived from organic matter sources, but a fraction of the methane results from conversion DIC generated by AOM back to methane, via secondary carbonate reduction (CR). Box model results show that sites characterized by a high flux of methane gas from deeper sources support highest rates of methane consumption (by AOM) and of methane generation (by CR). At low flux sites, the microbial filter removes nearly all of the available dissolved methane, but only a small fraction of methane is consumed by microbes at high-flux sites.

In a recently submitted paper (Yao et al., 2018) report on a rare observation of a mini-fracture in near-surface sediments (30 cm below the seafloor) visualized by using rotational scanning X-ray of a core recovered from the Lomvi pockmark, Vestnesa Ridge west of Svalbard (1200 m water depth). Porewater geochemistry and lipid biomarkers signatures revealed clearly differences in the geochemical and biogeochemical regimes of this core compared with two additional ones recovered from pockmarks in Vestnesa Ridge, which we attribute to differential methane transport mechanisms. Our study suggests that mini-fractures facilitate important pathways for advective fluid and gas transport in surface sediment, thereby generating hotspots of AOM.

4.3 PRINS KARLS FORELAND

The upper edge of gas hydrate stability (UEGHS) was thought to be especially susceptible to changes in bottom water temperature that may result in an anthropogenically-driven release of methane. The report of numerous gas flares emanating from the seafloor at the depth of gas hydrate stability, was heralded as an indicator of anthropogenically-driven methane release from gas hydrate dissociation (Westbrook et al., 2009). Our results from water column surveys indicate that methane discharge in this region is not necessarily associated with the UEGHS, rather appears to be controlled by methane escape along at regional fault (Mau et al., 2017). Drilling in the region of postulated recent gas hydrate destabilization during MSM057, recovered no gas hydrate. Furthermore, geochemical changes observed in the boreholes were used by Wallmann et al. (2017) to document a marine regression during the Holocene, with a resulting drop in hydrostatic pressure that induced gas hydrate dissociation. Using output from transport-reaction and isostatically-coupled ice sheet models, this paper documents that the chloride depletion observed in the slope cores can be better explained by gas hydrate dissociation triggered by isostatic rebound. Furthermore, this analyses indicate that gas hydrates destabilization is not a significant source for gas emanating at the seabed.

4.4 STORJORDENA

The HFZ was proposed to serve as a pathway for methane transport, based on multiple gas seepage sites observed from 72⁰ to 79⁰ N that coincide with this structural lineament (Mau et al., 2017). Following the path of this structural feature, a group of mound-structures bearing gas hydrate was discovered in ~380 meters water depth in the Storfjordrenna Trough area (Figure 9). As documented in Hong et al. (2017), cores recovered from these gas hydrate mounds (GHM) contain abundant methane-derived authigenic carbonate nodules. At sites with active gas discharge, gas hydrates occurred as shallow as 0.85 meters below seafloor (mbsf). Dating of two planktonic foraminifera specimens from a 3.2 m long core without any sign of active methane discharge yield an age for the bottom of this core slightly
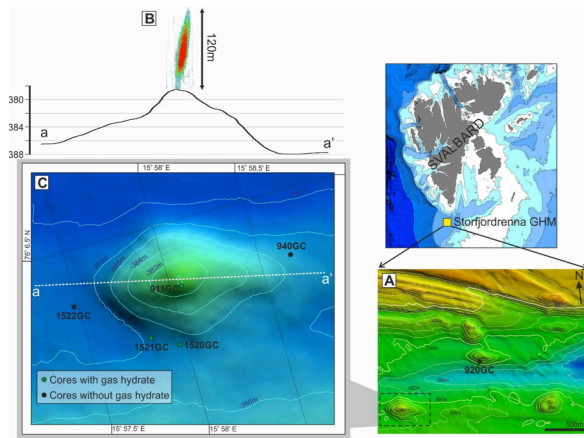
Figure 9. Bathymetry and core location of a Storfjordrenna gas hydrate mound. (A) Bathymetry of the general area of Storfjordrenna GHM. We recovered gas hydrates from three of the study sites (green dots). 920GC in the inset map shows the location of a site steady-state porewater profiles (Figure 3). Detailed bathymetry of the studied GHM is shown in (C) with the transect aa' line shown in (B) where the hydroacoustic flare was observed limited to the summit of the mound From Hong et al., 2017..

older than 16.2 kyrBP whereas the upper 70 cm is of Holocene age (Hong et al., 2017)

Since our originally proposed location at the PKF sites yielded no gas hydrate occurrence, we focus our study at these sites where gas hydrates occur at the UEGHS. The aim of our first paper at this location was is to investigate current and past seepage activities through the observations of porewater and sediments (Hong et al., 2017). We use porewater sulfate profiles as a proxy for the activity of anaerobic oxidation of methane (AOM), which responses to the supply of methane from greater depth. The obtained sulfate profiles exhibit concave-up shapes, an indication of an evolving and dynamic porewater system that was investigated using a transport-reaction model. This analysis was complemented with a study of authigenic carbonate nodules recovered at various GHMs to elucidate the mechanisms that modulate seepage strength (Figure 10). We discussed two competing hypotheses: shallow gas hydrate dissociation due to bottom water warming and episodic methane release controlled by geological factors (e.g., reservoir activities and fracture development). Bottom water warming may induce gas hydrate destabilization and trigger a concomitant increase of methane supply from the sediments. Alternatively, ongoing and past methane emission events may reflect episodic ventilation of a fluid reservoir that is controlled by the activity of gas reservoirs and the episodic opening of fluid conduits. Based on the data and model results we conclude that methane discharge, and consequently gas hydrate formation is driven by geodynamic properties of the system and does not respond in any significant way to changes in bottom water temperature.

Further analyses of geochemical data collected at the GHMs allowed us to construct a three-stage evolution model for active seepage in the region where gas hydrates are present in the shallow subsurface presented in Hong et al., 2018. In this model, a pre-active stage, solute diffusion is the primary mechanism for methane in the dissolved phase. Diffusion is also revealed by radiogenic strontium values that reflect silicate weathering in the microbial methanogenesis zone. During the active seepage stage, migration of gaseous methane results in the near-seafloor gas hydrate formation and vigorous seafloor discharge of gas with a thermogenic fingerprint. In the post-active seepage stage, the high concentration of dissolved
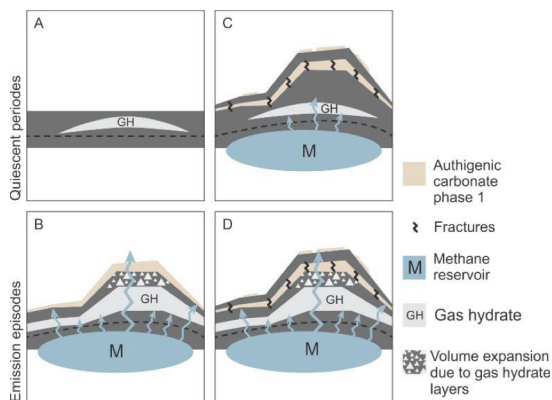
Figure 10 Proposed evolution of Storfjordrenna gas hydrate mounts. We identified several layers of authigenic carbonates indicating distinct seepage events. The fine hemipelagic sediments between the carbonate layers represent quiescent periods with weak methane supply. Non-steady state sulfate profiles signal an increase in methane supply within the sediments. These ongoing and past seepage events are interpreted as being induced by the ventilation of the gas reservoir at depth.

lithium points to the contribution of a deeper-sourced aqueous fluid, which we postulate advects upwardly following cessation of gas discharge. Different mounds represent different stages of seep evolution, consistent with our postulate that methane flux is not controlled by regional forcings (e.g. temperature), but localized dynamics of methane venting.

Because gas hydrate-rich seafloor mounds at Storfjordrenna are experiencing different methane flux regimes ranging from diffusive transport to active gas advection, we selected this location to investigate the microbial response to changes in methane flux, which was one of the objectives of the proposal. Results from an integrated microbial/geochemical study was recently submitted for publication (Klasek et al., 2018). This study show that populations of anaerobic methanotrophs and sulfate-reducing bacteria were highest at a seep site, and recent methane influx was associated with decreased community diversity. After fronts of methane passed through sediment depths and starved communities of sulfate, their structures shifted on timescales of years. Despite high methane fluxes and methanotroph doubling times of 5-9 months, microbial responses are largely synchronous with the advancement of the methane front. Our integrated approach of analyzing microbial community data within the context of geochemical and temporal gradients, allowed for a richer understanding of microbial ecology in response to changes in methane flux at seep sites.

The observations based on natural systems were further complemented with laboratory incubation data. Marine sediments were collected from one of the gas hydrate-bearing mounds offshore Svalbard were incubated for varying times at *in situ* temperature (4°C) and pressure (4.0 MPa) under different methane concentrations to investigate how methane structures microbial communities and whether rates of sulfate-dependent anaerobic methane oxidation (AOM) are linked with community changes. Sulfate reduction rates increased, and dissolved inorganic carbon isotopes became lighter during later stages of longer (4-8 month) incubations with added methane, indicating that AOM was established. This effect was only seen in sediments collected from methane-rich areas, suggesting that longer times or higher methane concentrations are needed to stimulate AOM in methane-naïve sediments. However, concentrations of the methane-fixing *mcrA* gene did not notably increase in these enrichments. Methane-naïve sediment

communities changed more drastically than sediments from methane-rich areas, though these changes were not methane-dependent. They may instead reflect that over months-long timescales, AOM activity precedes large-scale microbial community changes, particularly the growth of anaerobic methanotrophs, in marine sediments. A manuscript detailing these results in in preparation (Klasek et al., in prep).

5. CONCLUSIONS:

The landward termination of gas hydrate stability along continental slopes worldwide is thought to be susceptible to changes in bottom water temperature that may result in an anthropogenically-driven release of methane. The report of numerous gas plumes emanating from the seafloor offshore Prins Karls Forland, was presented by Westbrook et al (2009) as evidence for gas hydrate dissociation driven by an increase in intermediate water temperature over the past 30 years. Hydroacoustic records indicative of gas discharge on the North American Atlantic continental slope and along the Cascadia margin have also been tied to gas hydrate destabilization at the landward edge of their stability zone. These postulated gas hydrate destabilization events have been proposed by Johnson et al. (2015) to have far-reaching consequences, including oxygen consumption, pH changes harmful to benthic biota, tsunami-generating slope failures, and climate feedbacks that enhance global warming. The various aspects of the research conducted under this grant consistently point the conclusion that methane seepage observed the Svalbard margin is not related to a temperature-induced destabilization of gas hydrate, rather the methane release is controlled by tectonic, geologic and reservoir dynamics. The conclusion that the release of methane from hydrate decomposition is a small component of overall methane input along ocean margins and, more significantly, that the methane currently observed as plumes along continental slopes is not a new phenomenon fueled by anthropogenic change are stated in the Fire in the Ice (volume 17, issue 2) article by Mau et al (2017). Below we summarize these ideas, and complement them with more recent findings.

Our water column surveys identified a large Svalbard plume along the trace of the HFS, with many of the seeps located at and above the gas hydrate stability zone. We conclude that large methane plumes such as the Svalbard plume appear to be natural phenomena, not associated with gas hydrate dynamics. Our data show that gas flares feeding the shallower than ~120 m extend from the seafloor to the sea surface. Highest dissolved methane concentrations were measured above the shallow seeps off PKF, Hornsundbanken, and Soerkappbanken, with values reaching 878 nM above atmospheric equilibrium. High supersaturation values during summer surveys lead to highs in sea-air fluxes of up to 2.0 nmol m^{-2} s^{-1}. The increase in wind speeds during the winter months may increase this flux, as has been demonstrated for natural seeps in the central North Sea. It remains unclear whether atmospheric methane anomalies measured in the 2015 surveys represent direct input from the shallow mapped seeps, from seeps closer to land, or even from methane discharge on the island itself. Nonetheless, the supersaturation values

consistently measured in the upper 10 m of stations closer to the shelf point to some contribution to the atmosphere from the shallow portion of the Svalbard plume.

Consistent with the inferences based on water column data, drilling at the PFK slope showed that gas hydrates are not present in this area, thus negating the postulate that destabilization of gas hydrate is responsible for the methane release (Wallmann et al., 2018). Two other important conclusions result from this study: 1) gas hydrate was present in the region during the last glacial period, and destabilization of these deposits was induced by isostatic rebound processes following retreat of the Barents ice sheet; and 2) even during this destabilization event, no significant amount of methane was released to the water column.

Another investigation of the role of temperature in gas hydrate stability was conducted at a location where gas hydrate mounds were found to occur at the upper edge of gas hydrate stability in Storfjordrenna, just south of Spitzbergen (Hong et al., 2017). Analyses of the effect of temperature changes at this site revealed that not to be a significant control on the gas flux dynamics, rather the system is controlled by localized variations in gas reservoirs dynamics that result in a stage-wise release and accumulation of subsurface gas (Hong et al., 2018). In addition, these studies: 1) documented episodicity of the methane release episodes that span time periods much longer than any anthropogenic forcing and 2) provide constraints for modeling assessments of future warming scenarios on the stability of Arctic gas hydrate reservoirs and the postulated methane release.

Other significant results focus on the role of microbial activity on carbon cycling at sites with significant methane fluxes. Because archaea performing anaerobic methane oxidation (AOM) prevent methane produced in marine sediments from reaching the hydrosphere, it is important to characterize their response to changing methane fluxes. We show that a significant portion of the inorganic carbon generated during AOM is converted back to methane at or immediately below the SMT (Pape et al., 2018). Using data and modeling approaches we quantified the AOM rates and the amount of methane sequestered in authigenic carbonate as a function of methane flux. We show that sites with methane gas discharge support higher AOM rates. Furthermore, through integrated microbial, geochemical and modeling approach we were able to conclude that 1) recent seepage supports the growth of high populations of anaerobic methanotrophs and sulfate-reducing bacteria, 2) the establishment of a sulfate-methane transition zone constrains the depth and number of these groups as methane flux increases into shallower layers, and 3) community diversity rebounds as steady-state sulfate-methane dynamics are reached (Klasek et al., 2018). Cold seeps are dynamic systems with temporal perturbations in methane flux.

Based on our collective new understanding from this comprehensive research effort we postulate that it is likely that little, if any, of the methane discharge events along continental slopes is directly tied to anthropogenic forcing. Seepage at these locations is instead part of a continental margin-wide set of processes that respond to hydrogeologic mechanisms. Our data and model results also strongly suggest that gas hydrates are not a significant source for gas emanating at the seabed. Rather,

they act as a dynamic seal that blocks fluid-flow pathways for gas ascent from deep geological reservoirs. Previous estimates of methane release by ongoing and future gas hydrate decomposition consider gas release from hydrates but ignore the potentially more significant increase in flux from underlying gas reservoirs. Hence, the impact of future seabed methane fluxes on global environmental change may be underestimated, and further research is required to quantify the release from deep natural gas reservoirs induced by deterioration of the overlying hydrate seal.

Whereas massive methane release from a recently triggered gas hydrate destabilization methane release along continental slopes does not contribute to the atmosphere, it is important to evaluate the potential sea-air flux from natural seeps along the continental shelves; where new evidence suggest there may be a contribution to atmospheric inventories driven by natural causes.

To better understand the role of subseafloor methane it is key to characterize the microbiological response to changes in environmental conditions, including variations in methane fluxes. Our results highlight the importance of framing microbial community data and estimates of their metabolic processes within a spatially and temporally constrained geochemical context to more thoroughly understand microbial contributions in structuring habitats and mediating biogeochemical cycles.

6. ACKNOWLEDGEMENTS

7. REFERENCES

Berndt, C. et al. Temporal Constraints on Hydrate-Controlled Methane Seepage off Svalbard. Science **343**, 284-287, doi:10.1126/science.1246298 (2014).

Bohrmann, G., F. Ahrlich, M. Bergenthal, S. Bünz, R. Düßmann, C. dos Santos Ferreira, et al. (2017), R/V MARIA S. MERIAN Cruise Report MSM57, Gas Hydrate Dynamics at the Continental Margin of Svalbard, Reykjavik – Longyearbyen – Reykjavik, 29 July – 07 September 2016., Berichte, MARUM - Zentrum für Marine Umweltwissenschaften, Fachbereich Geowissenschaften, Universität Bremen: Bremen, 204. doi:ISSN 2195-9633.

Boetius, Antje, and Frank Wenzhöfer. "Seafloor oxygen consumption fuelled by methane from cold seeps." *Nature Geoscience* 6.9 (2013): 725.

Boudreau, B. P. Diagenetic models and their implementation: modeling transport and reactions in aquatic sediments. 414 (Springer, 1997).

Bunz, S., Petersen, J., Hustoft, S., & Mienart, J. (2008). Environmentally-sensitive gas hydrates on the W-Svalbard margin at the gateway to the Arctic ocean.

Bussmann, I., Matousu, A., Osudar, R., & Mau, S. (2015). Assessment of the radio 3H-CH4 tracer technique to measure aerobic methane oxidation in the water column. Limnology and Oceanography: Methods, 13(6), 312-327.

Caporaso, J. G. et al. Global patterns of 16S rRNA diversity at a depth of millions of sequences per sample. Proceedings of the National Academy of Sciences **108,** 4516–4522 (2011).

Cline, J. D. Spectrophotometric Determination of Hydrogen Sulfide in Natural Waters. Anal. Chem **21**, 1005-1009 (1969).

Cremiere, A. et al. Timescales of methane seepage on the Norwegian margin following collapse of the Scandinavian ice sheet. Nature communication (2016).

EPA, C. EPA 600/4-79-020 METHODS FOR CHEMICAL ANALYSIS OF WATER AND WASTES <http://www.wbdg.org/ffc/epa/criteria/epa-600-4-79-020> (1983).

Evans, J., Sheneman, L. & Foster, J. Relaxed Neighbor Joining: A Fast Distance-Based Phylogenetic Tree Construction Method. J Mol Evol **62,** 785–792 (2006).

Excoffier, L., Smouse, P. E. & Quattro, J. M. Analysis of molecular variance inferred from metric distances among DNA haplotypes: application to human mitochondrial DNA restriction data. Genetics **131,** 479–491 (1992).

Fornari, D. J. (2003). A new deep-sea towed digital camera and multi-rock coring system. Eos, Transactions American Geophysical Union, 84(8), 69-73.

Freudenthal, T., and G. Wefer (2013), Drilling cores on the sea floor with the remote-controlled sea floor drilling rig MeBo, Geosci. Instrum. Meth., 2, 329-337, doi:10.5194/gi-2-329-2013.

Hong, W.-L., S. Sauer, G. Panieri, W. G. Ambrose, R. H. James, A. Plaza-Faverola, and A. Schneider (2016), Removal of methane through hydrological, microbial, and geochemical processes in the shallow sediments of pockmarks along eastern Vestnesa Ridge (Svalbard), Limnol. Oceanogr., 61, S324-S343, doi:10.1002/lno.10299.

Hong, W.-L., Solomon, E. A. & Torres, M. E. A kinetic-model approach to quantify the effect of mass transport deposits on pore water profiles in the Krishna–Godavari basin, Bay of Bengal. Marine and Petroleum Geology (2014).

Hong, W.-L., Torres, M. E., Kim, J.-H., Choi, J. & Bahk, J.-J. Towards quantifying the reaction network around the sulfate–methane-transition-zone in the Ulleung Basin, East Sea, with a kinetic modeling approach. Geochim. Cosmochim. Acta **140**, 127-141, doi:http://dx.doi.org/10.1016/j.gca.2014.05.032 (2014).

Hong, W. L., Torres, M. E., Carroll, J., Crémière, A., Panieri, G., Yao, H., & Serov, P. (2017). Seepage from an arctic shallow marine gas hydrate reservoir is insensitive to momentary ocean warming. Nature communications, 8, 15745.10.1038/NCOMMS15745.

Hong, W. L., Torres, M. E., Portnov, A., Waage, M., Haley, B., & Lepland, A. (2018). Variations in gas and water pulses at an Arctic seep: fluid sources and methane transport. *Geophysical Research Letters*, *45*(9), 4153-4162.

Hustoft, S., Bünz, S., Mienert, J., & Chand, S. (2009). Gas hydrate reservoir and active methane-venting province in sediments on< 20 Ma young oceanic crust in the Fram Strait, offshore NW-Svalbard. *Earth and Planetary Science Letters*, *284*(1-2), 12-24.

Johnson, H. P., Miller, U. K., Salmi, M. S., & Solomon, E. A. (2015). Analysis of bubble plume distributions to evaluate methane hydrate decomposition on the continental slope. *Geochemistry, Geophysics, Geosystems*, *16*(11), 3825-3839.

Joseph, C., Torres, M. E., Martin, R. A., Haley, B. A., Pohlman, J. W., Riedel, M., & Rose, K. (2012). Using the 87 Sr/86 Sr of modern and paleoseep carbonates from northern Cascadia to link modern fluid flow to the past. *Chemical Geology*, *334*, 122-130.

Joseph, C., Campbell, K. A., Torres, M. E., Martin, R. A., Pohlman, J. W., Riedel, M., & Rose, K. (2013). Methane-derived authigenic carbonates from modern and paleoseeps on the Cascadia margin: Mechanisms of formation and diagenetic signals. *Palaeogeography, Palaeoclimatology, Palaeoecology*, *390*, 52-67.

Klasek, S. W-L.Hong, M. E. Torres, S. Ross, K. Hostetler, A. Portnov, F. Gründger, F. S. Colwell. Methane-driven microbial community succession in Arctic seafloor gas hydrate mounds. Submitted to Nature communications on 9/18/18 (reference number: NCOMMS-18-28379)

Kondo, R., Nedwell, D. B., Purdy, K. J. & Silva, S. Q. Detection and Enumeration of Sulphate-Reducing Bacteria in Estuarine Sediments by Competitive PCR. Geomicrobiology Journal **21,** 145–157 (2004).

Kozich, J. J., Westcott, S. L., Baxter, N. T., Highlander, S. K. & Schloss, P. D. Development of a Dual-Index Sequencing Strategy and Curation Pipeline for Analyzing Amplicon Sequence Data on the MiSeq Illumina Sequencing Platform. Appl Environ Microbiol **79,** 5112–5120 (2013).

Lozupone, C. A., Hamady, M., Kelley, S. T. & Knight, R. Quantitative and Qualitative β Diversity Measures Lead to Different Insights into Factors That Structure Microbial Communities. Appl. Environ. Microbiol. **73,** 1576–1585 (2007).

Luton, P. E., Wayne, J. M., Sharp, R. J. & Riley, P. W. The mcrA gene as an alternative to 16S rRNA in the phylogenetic analysis of methanogen populations in landfillb. Microbiology **148,** 3521–3530 (2002).

Magen, C., Lapham, L. L., Pohlman, J. W., Marshall, K., Bosman, S., Casso, M., & Chanton, J. P. (2014). A simple headspace equilibration method for measuring dissolved methane. Limnology and Oceanography: Methods, 12(9), 637-650.

Mau, S., Römer, M., Torres, M.E., Bussmann, I., Pape, T., Damm, E., Geprägs, P., Wintersteller, P., Hsu, C.W., Loher, M. and Bohrmann, G., 2017. Widespread methane seepage along the continental margin off Svalbard-from Bjørnøya to Kongsfjorden. Scientific Reports, 7.

Mau, S., Torres, M.E., Römer, M, Pape, T. and Bohrmann, G. (2017b) Methane release along continental margins: natural process or anthropogenically driven?, Fire in the Ice, 17 (2), 5-8.

Panieri, G., S. Bünz, D. J. Fornari, J. Escartin, P. Serov, P. Jansson, et al. (2017), An integrated view of the methane system in the pockmarks at Vestnesa Ridge, 79°N, Mar. Geol., 390, 282-300, doi:10.1016/j.margeo.2017.06.006.

Panieri, G., D. J. Fornari, P. Serov, E. K. L. Åström, A. Plaza-Faverola, J. Mienert, et al. (2015), Gas hydrate, carbonate crusts, and chemosynthetic organisms on a Vestnesa Ridge pockmark - preliminary findings, Fire in the Ice, 15(2), 14-17.

Pape, T., A. Bahr, J. Rethemeyer, J. D. Kessler, H. Sahling, K. U. Hinrichs, et al. (2010), Molecular and isotopic partitioning of low-molecular weight hydrocarbons during migration and gas hydrate precipitation in deposits of a high-flux seepage site, Chem. Geol., 269(3-4), 350-363, doi:10.1016/j.chemgeo.2009.10.009.

Pape, T. S. Bünz, W.-L. Hong, M.E. Torres, M. Riedel, G. Panieri, A. Lepland, C.W. Hsu, P. Wintersteller, K. Wallmann, C. Schmidt, H. Yao, and G. Bohrmann. Origin and transformation of light hydrocarbons ascending at an active pockmark on Vestnesa Ridge, Arctic Ocean. Submitted to Journal of Geophysical Research - Solid Earth on 9/10/18 (reference number 2018JB016679).

Plaza-Faverola, A., S. Bünz, J. E. Johnson, S. Chand, J. Knies, J. Mienert, and P. Franek (2015), Role of tectonic stress in seepage evolution along the gas hydrate-charged Vestnesa Ridge, Fram Strait, Geophys. Res. Lett., 42(3), 733-742, doi:10.1002/2014gl062474.

Plaza-Faverola, A., S. Vadakkepuliyambatta, W. L. Hong, J. Mienert, S. Bünz, S. Chand, and J. Greinert (2017), Bottom-simulating reflector dynamics at Arctic thermogenic gas provinces: An example from Vestnesa Ridge, offshore west Svalbard, J. Geophys. Res.-Sol.Ea., 122(6), 4089-4105, doi:10.1002/2016JB013761.

Peszynska, M., Medina, F.P., Hong, W.L. and Torres, M.E., 2015. Reduced Numerical Model for Methane Hydrate Formation under Conditions of Variable Salinity. Time-Stepping Variants and Sensitivity. Computation, 4(1), p.1.

Peszynska, M., Hong, W.L. Torres, M.E., and Kim, J-H., 2015. Methane Hydrate Formation in Ulleung Basin Under Conditions of Variable Salinity: Reduced

Model and Experiments. Transport Porous Media DOI 10.1007/s11242-016-0706-y

Petersen, C. J., Bünz, S., Hustoft, S., Mienert, J., & Klaeschen, D. (2010). High-resolution P-Cable 3D seismic imaging of gas chimney structures in gas hydrated sediments of an Arctic sediment drift. *Marine and Petroleum Geology*, *27*(9), 1981-1994.

Sahling, H. et al. Gas emissions at the continental margin west off Svalbard: mapping, sampling, and quantification. Biogeosciences Discussions **11**, 7189-7234 (2014).

Salter, S. J. et al. Reagent and laboratory contamination can critically impact sequence-based microbiome analyses. BMC Biology **12,** 87 (2014).

Schloss, P. D. et al. Introducing mothur: Open-Source, Platform-Independent, Community-Supported Software for Describing and Comparing Microbial Communities. Appl. Environ. Microbiol. **75,** 7537–7541 (2009).

Sloan Jr, E. D. & Koh, C. Clathrate hydrates of natural gases. third edn, (CRC press, 2008).

Steefel, C. et al. Reactive transport codes for subsurface environmental simulation. Computational Geosciences, 1-34 (2014).

Quast, C. et al. The SILVA ribosomal RNA gene database project: improved data processing and web-based tools. Nucleic Acids Res **41,** D590–D596 (2013).

Torres, M. E., A. C. Mix, and W. D. Rugh (2005), Precise $\delta^{13}C$ analysis of dissolved inorganic carbon in natural waters using automated headspace sampling and continuous-flow mass spectrometry, Limnology and Oceanography Methods, 3, 349-360, doi:10.4319/lom.2005.3.349.

Vanneste, M., S. Guidard, and J. Mienert (2005), Bottom-simulating reflections and geothermal gradients across the western Svalbard margin, Terra Nova, 17(6), 510-516, doi:10.1111/j.1365-3121.2005.00643.x.

Vogt, P. R., K. Crane, E. Sundvor, M. D. Max, and S. L. Pfirman (1994), Methane-generated(?) pockmarks on young, thickly sedimented oceanic crust in the Arctic: Vestnesa ridge, Fram strait, Geology, 22, 255-258, doi:10.1130/0091-7613(1994)022<0255:MGPOYT>2.3.CO;2.

Vogt, P. R., J. Gardner, and K. Crane (1999), The Norwegian-Barents-Svalbard (NBS) continental margin: Introducing a natural laboratory of mass wasting, hydrates, and ascent of sediment, pore water, and methane, Geo-Mar. Lett., 19(1 - 2), 2-21, doi:10.1007/s003670050088.

Vorren, T. O., Hald, M., & Lebesbye, E. (1988). Late cenozoic environments in the Barents Sea. *Paleoceanography and Paleoclimatology*, *3*(5), 601-612.

Wallmann, K., M. Riedel, W. L. Hong, H. Patton, A. Hubbard, T. Pape, et al. (2018), Gas hydrate dissociation off Svalbard induced by isostatic rebound rather than global warming, Nat. Commun., 9(1), 83, doi:10.1038/s41467-017-02550-9.

Westbrook, G. K. et al. Escape of methane gas from the seabed along the West Spitsbergen continental margin. Geophysical Research Letters **36**, doi:L15608 10.1029/2009gl039191 (2009).

White, J. R., Nagarajan, N. & Pop, M. Statistical Methods for Detecting Differentially Abundant Features in Clinical Metagenomic Samples. PLoS Comput Biol **5,** (2009).

Yao, H. W-L. Hong, G. Panieri, S. Sauer, M. E. Torres, M. F. Lehmann, F. Gründger and H. Niemann. Fracture-controlled fluid transport supports microbial methane-oxidizing communities at the Vestnesa Ridge. Submitted to Biogeosciences, June 2018

8. PUBLICATIONS RESULTING FROM THIS PROJECT

8.1 PEER-REVIEWED PAPERS

Peszynska, M., Medina, F.P., Hong, W.L. and Torres, M.E., 2015. Reduced Numerical Model for Methane Hydrate Formation under Conditions of Variable Salinity. Time-Stepping Variants and Sensitivity. Computation, 4(1), p.1.

Peszynska, M., Hong, W.L. Torres, M.E., and Kim, J-H., 2015. Methane Hydrate Formation in Ulleung Basin Under Conditions of Variable Salinity: Reduced Model and Experiments. Transport Porous Media DOI 10.1007/s11242-016-0706-y

Mau, S., Römer, M., Torres, M.E., Bussmann, I., Pape, T., Damm, E., Geprägs, P., Wintersteller, P., Hsu, C.W., Loher, M. and Bohrmann, G., 2017. Widespread methane seepage along the continental margin off Svalbard-from Bjørnøya to Kongsfjorden. Scientific Reports, 7.

Hong, W. L., Torres, M. E., Carroll, J., Crémière, A., Panieri, G., Yao, H., & Serov, P. (2017). Seepage from an arctic shallow marine gas hydrate reservoir is insensitive to momentary ocean warming. Nature communications, 8, 15745.10.1038/NCOMMS15745.

Panieri G, Bünz S, Fornari DJ, Escartin J, Serov P, Jansson P, Torres ME, Johnson JE, Hong W, Sauer S, Garcia R. An integrated view of the methane system in the pockmarks at Vestnesa Ridge, 79° N. Marine Geology. 2017 Aug 1;390:282-300.

Wallmann K, Riedel M, Hong WL, Patton H, Hubbard A, Pape T, Hsu CW, Schmidt C, Johnson JE, Torres ME, Andreassen K. Gas hydrate dissociation off Svalbard induced by isostatic rebound rather than global warming. Nature Communications. 2018 Jan 8;9(1):83.

Hong, W. L., Torres, M. E., Portnov, A., Waage, M., Haley, B., & Lepland, A. (2018). Variations in gas and water pulses at an Arctic seep: fluid sources and methane transport. *Geophysical Research Letters*, *45*(9), 4153-4162.

8.2 SUBMITTED PAPERS

Scott A. Klasek, WeiLi Hong, Marta E. Torres, Stella Ross, Katelyn Hostetler, Alexey Portnov, Friederike Gründger, Frederick S. Colwell. Methane-driven

microbial community succession in Arctic seafloor gas hydrate mounds. Submitted to Nature communications on 9/18/18 (reference number: NCOMMS-18-28379)

T. Pape, S. Bünz, W.-L. Hong, M.E. Torres, M. Riedel, G. Panieri, A. Lepland, C.W. Hsu, P. Wintersteller, K. Wallmann, C. Schmidt, H. Yao, and G. Bohrmann. Origin and transformation of light hydrocarbons ascending at an active pockmark on Vestnesa Ridge, Arctic Ocean. Submitted to Journal of Geophysical Research - Solid Earth on 9/10/18 (reference number 2018JB016679).

Haoyi Yao, Wei-Li Hong, Giuliana Panieri, Simone Sauer, Marta E. Torres, Moritz F. Lehmann, Friederike Gründger and Helge Niemann Fracture-controlled fluid transport supports microbial methane-oxidizing communities at the Vestnesa Ridge. Submitted to biogeosciences, June 2018

8.3 MANUSCRIPT IN PREPARATION

Scott Klasek, WeiLi Hong, Marta Torres, Douglas Bartlett, Frederick Colwell. Methane drives activity before structure in microbial communities inhabiting marine sediment sulfate-methane interfaces. The results will be presented at the upcoming AGU meeting in Washington DC, Dec 2018

8.4 ARTICLES IN FIRE IN THE ICE

Panieri, G., D. J. Fornari, P. Serov, E. K. L. Åström, A. Plaza-Faverola, J. Mienert, et al. (2015), Gas hydrate, carbonate crusts, and chemosynthetic organisms on a Vestnesa Ridge pockmark - preliminary findings, Fire in the Ice, 15(2), 14-17.

Mau, S., Torres, M.E., Römer, M, Pape, T. and Bohrmann, G. (2017) Methane release along continental margins: natural process or anthropogenically driven?, Fire in the Ice, 17 (2), 5-8.

National Energy Technology Laboratory

626 Cochrans Mill Road
P.O. Box 10940
Pittsburgh, PA 15236-0940

3610 Collins Ferry Road
P.O. Box 880
Morgantown, WV 26507-0880

13131 Dairy Ashford Road, Suite 225
Sugar Land, TX 77478

1450 Queen Avenue SW
Albany, OR 97321-2198

Arctic Energy Office
420 L Street, Suite 305
Anchorage, AK 99501

Visit the NETL website at:
www.netl.doe.gov

Customer Service Line:
1-800-553-7681

NE NATIONAL
E ENERGY
TL TECHNOLOGY
LABORATORY

U.S. DEPARTMENT OF
ENERGY | NATIONAL ENERGY
TECHNOLOGY LABORATORY